Supporting Information

Structural Isomerism Effect in Platinum(II) Acetylide-Based Supramolecular Polymers

Ze Chen, Yuncong Xue, Mingliang Gui, Cong Wang, and Feng Wang*

CAS Key Laboratory of Soft Matter Chemistry, Department of Polymer Science and Engineering, University of Science and Technology of China, Hefei, Anhui 230026 P. R. China, E-mail: drfwang@ustc.edu.cn.

*1. Spectra of **1–2** at the monomeric state*

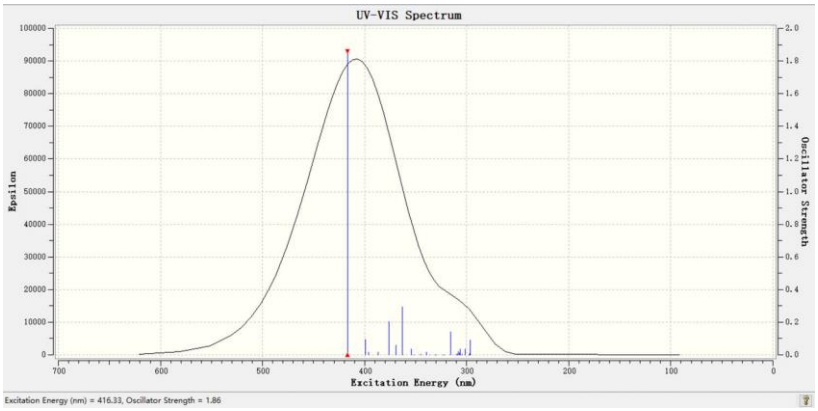

Figure S1. Simulated UV–Vis spectrum of **1** in chloroform *via* TD-DFT calculation.

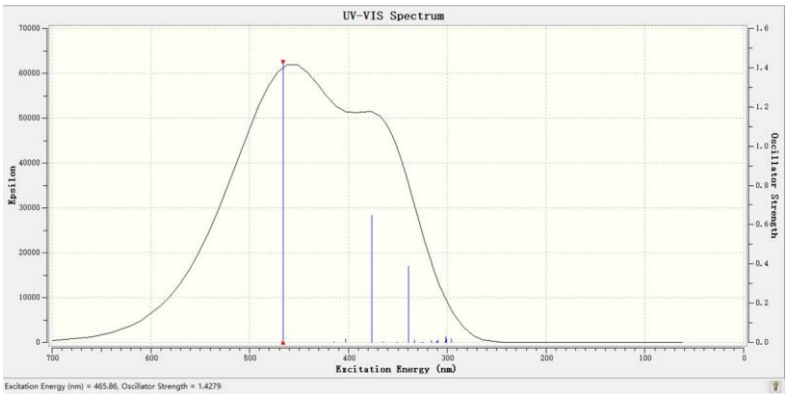

Figure S2. Simulated UV–Vis spectrum of **2** in chloroform *via* TD-DFT calculation.

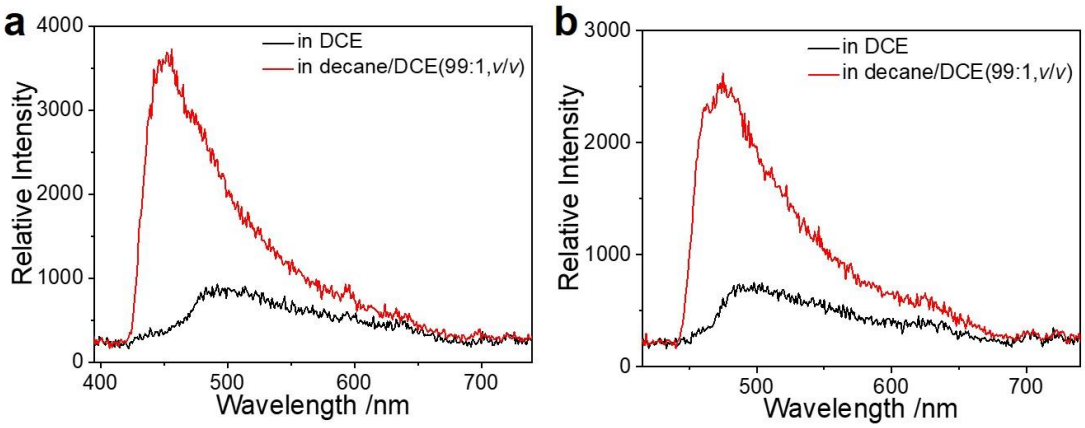

Figure S3. Emission spectra of (a) **1** (λ_{ex} = 380 nm) and (b) **2** (λ_{ex} = 420 nm) in 1,2-dichoroethane (black lines) and decane/1,2-dichoroethane (99 : 1, *v*/*v*) (red lines).

2. Supramolecular polymerization of ***2***

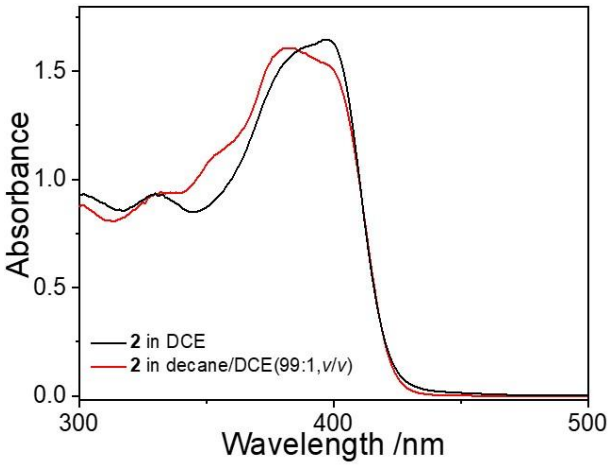

Figure S4. UV–Vis spectra of **2** (c = 0.05 mM, 293 K) in 1,2-dichoroethane and decane/1,2-dichoroethane (99 : 1, *v*/*v*). It shows slight hypochromic effect in the apolar medium [λ_{max}: from 420 in 1,2-dichloroethane to 416 nm in decane/1,2-dichloroethane (99 : 1, *v*/*v*)].

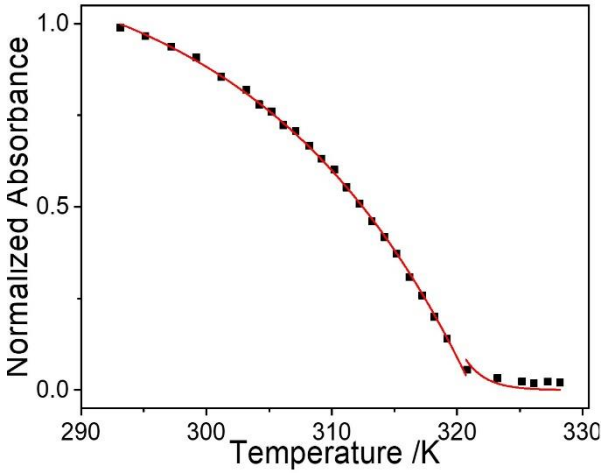

Figure S5. Normalized UV–Vis absorbance of **2** at 358 nm *versus* temperature upon heating (rate: 60 K h^{-1}). Condition: c = 0.05 mM, decane/1,2-dichoroethane (99 : 1, *v*/*v*), 5 mm cuvette. The solid lines denote Meijer–Schenning–van der Schoot mathematical model fitting of the curve.

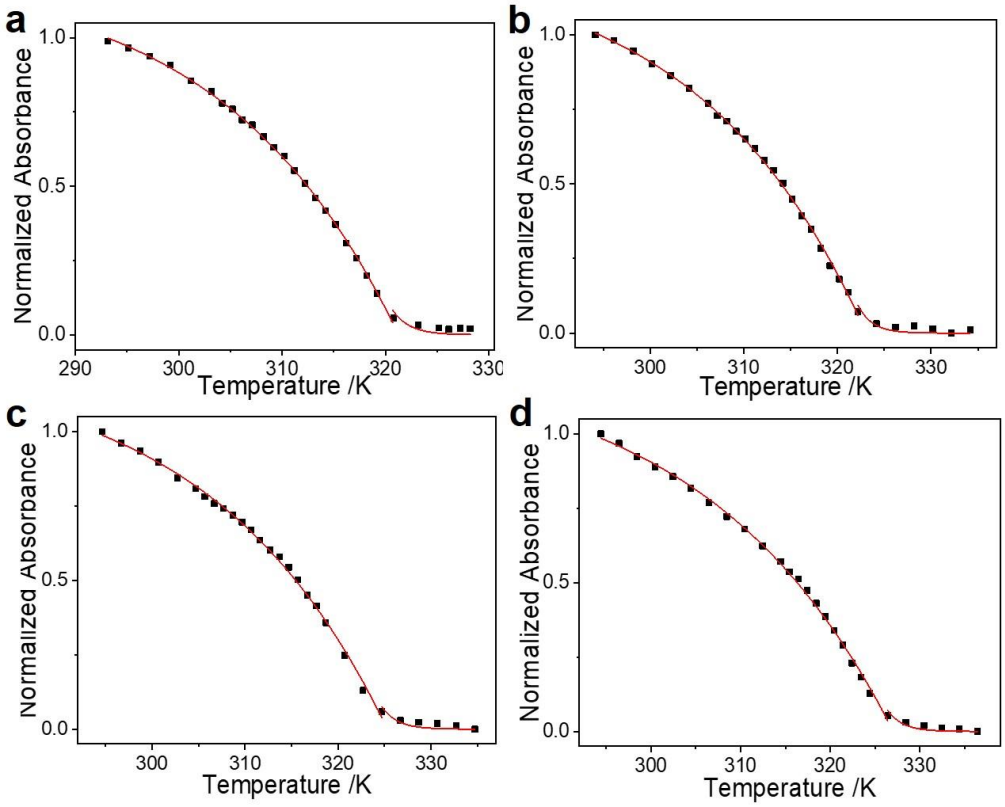

Figure S6. Normalized UV–Vis absorbance intensity of **2** at 358 nm in decane/1,2-dichoroethane (99 : 1, *v*/*v*) at different monomer concentration: a) 0.05 mM; b) 0.06 mM; c) 0.07 mM; d) 0.08 mM. The solid lines denote mathematical fitting of the curves by Meijer–Schenning–van der Schoot model. The quantitative thermodynamic values are shown in **Table S1**.

Table S1. **Thermodynamic parameters of 2 obtained by fitting temperature-dependent UV–Vis data.**

2	0.05 mM	0.06 mM	0.07 mM	0.08 mM
T_e (K)	320.8	323.1	325.3	327.0
h_e (kJ mol^{-1})	–53.1	–48.8	–46.5	–42.4

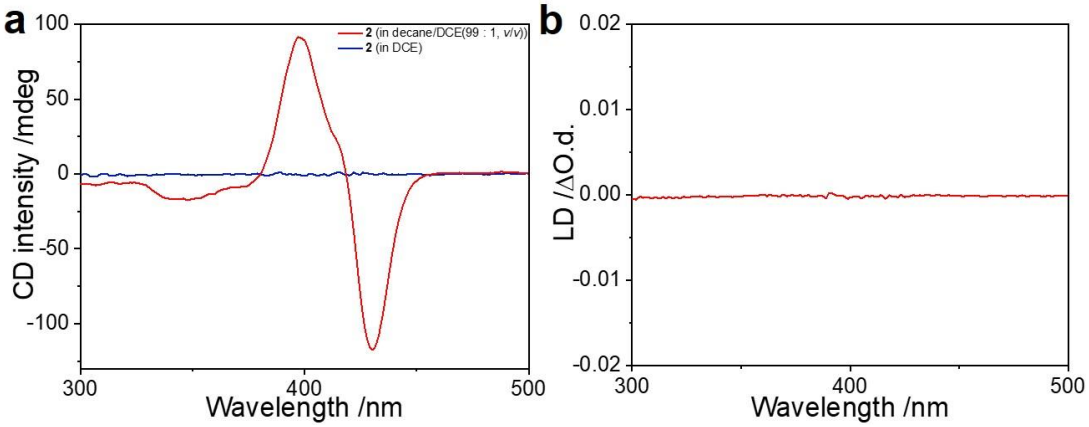

Figure S7. (a) CD spectra of **2** (c = 0.05 mM, 293 K, 5 mm cuvette) in 1,2-dichoroethane and decane/1,2-dichoroethane (99 : 1, *v*/*v*). (b) LD spectrum of **2** [0.05 mM in decane/1,2-dichoroethane (99 : 1, *v*/*v*), 293K]. As can be seen, no LD signal is detected, demonstrating the measured CD signals are real to reflect the supramolecular chirality.

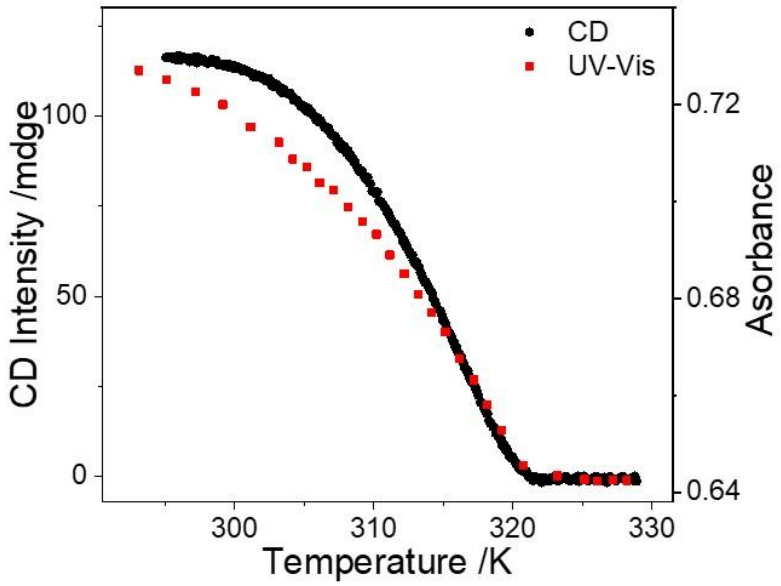

Figure S8. Overlapped normalized UV–Vis and CD intensity of **2** *versus* temperature in decane/1,2-dichoroethane (99 : 1, *v*/*v*, c = 0.05 mM) at a heating rate of 60 K h^{-1}.

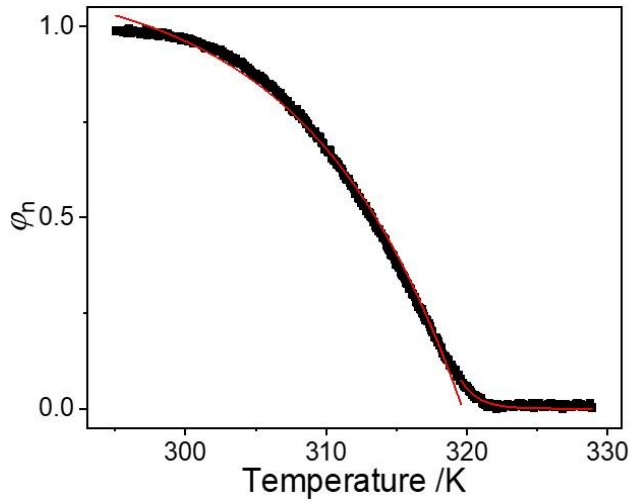

Figure S9. Normalized CD intensity of **2** *versus* temperature in decane/1,2-dichoroethane (99 : 1, *v*/*v*, *c* = 0.05 mM). The red solid lines denote the mathematical fitting of the melting curve by the Meijer–Schenning–van der Schoot mathematical model. The quantitative thermodynamic values are shown in **Table 1**.

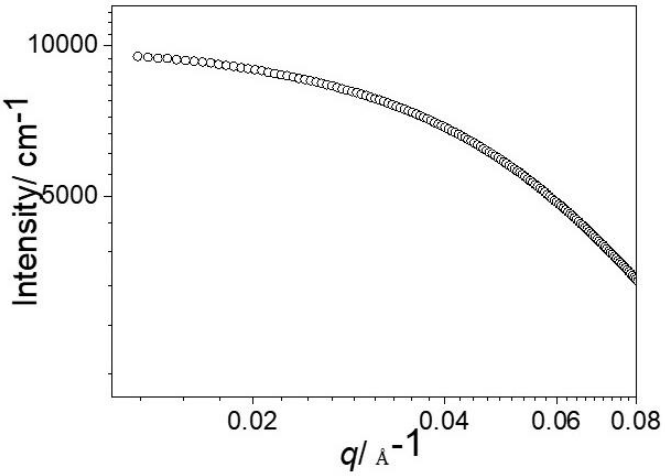

Figure S10. Plots of log I(*q*) *versus* log (*q*) of SAXS for **2** (0.10 mM in MCH). A q^{-1} slope is obtained in the region $0.03 < q < 0.08$ Å^{-1}, indicating the formation of one-dimensional rod-like structure upon supramolecular polymerization.

*3. Supramolecular polymerization of **1***

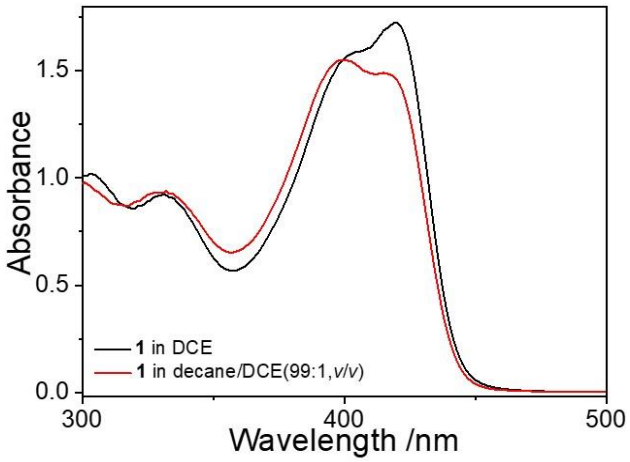

Figure S11. UV–Vis spectra of **1** (c = 0.05 mM, 293 K) in 1,2-dichoroethane and decane/1,2-dichoroethane (99 : 1, v/v).

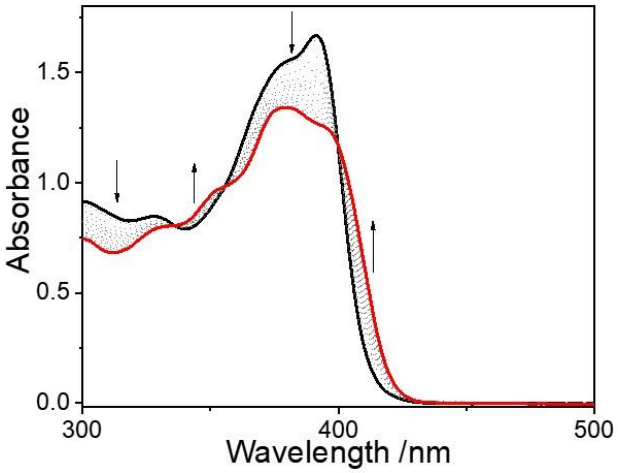

Figure S12. Temperature-dependent UV–Vis spectra of **1** (c = 0.05 mM) in decane/1,2-dichoroethane (99 : 1, v/v). The arrows show spectral changes upon increasing the temperature. Three isosbestic points are present (λ: 335, 355 and 399 nm) upon varying the temperature in decane/1,2-dichloroethane (99 : 1, v/v), supporting reversible conversion between the monomeric and aggregated states.

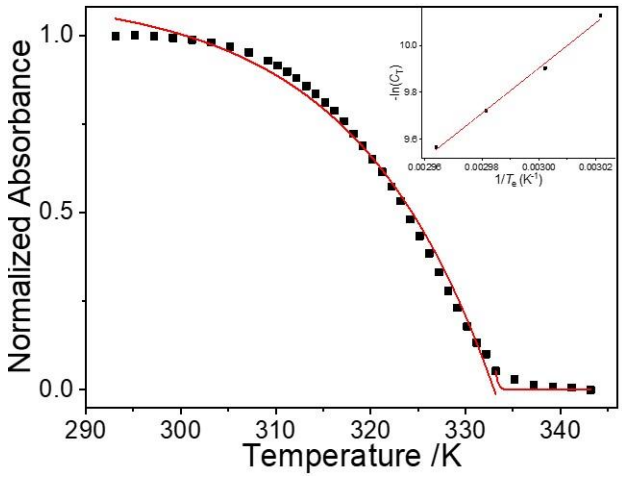

Figure S13. Normalized UV–Vis absorbance of **1** at 411 nm *versus* temperature upon heating (rate: 60 K h^{-1}). Condition: c = 0.05 mM, decane/1,2-dichoroethane (99 : 1, *v*/*v*), 5 mm cuvette. The solid lines denote Meijer–Schenning–van der Schoot mathematical model fitting of the curve. Inset: van't Hoff plot fitting of **1**. The concentration is made dimensionless by dividing 10^{-5} M.

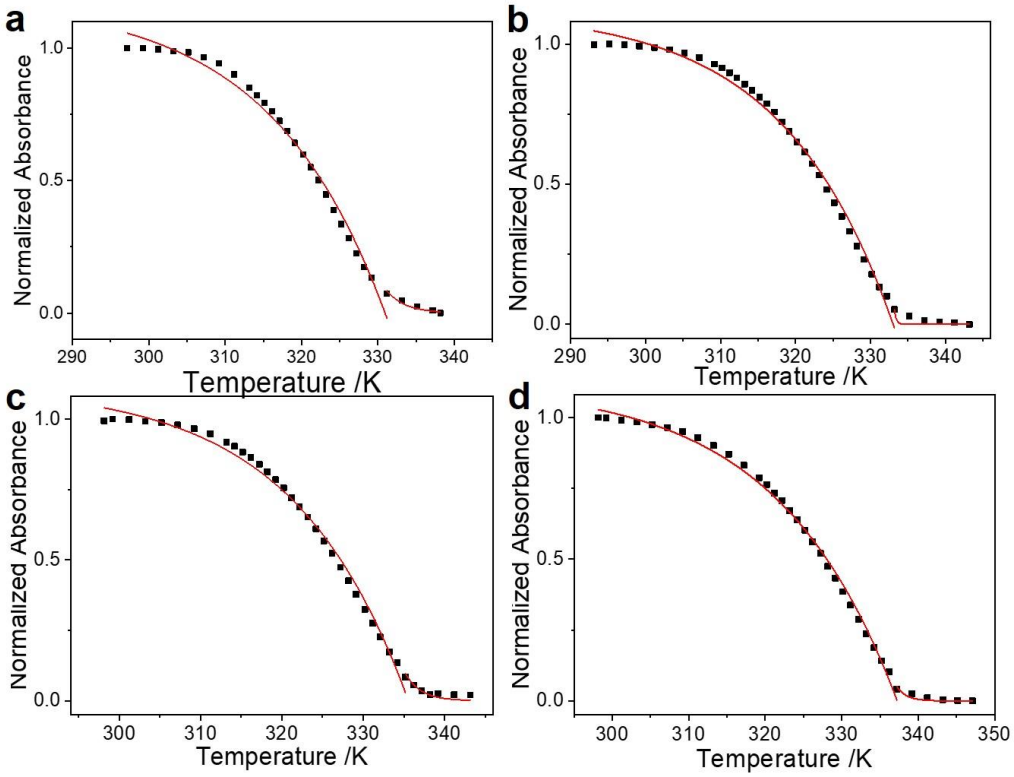

Figure S14. Normalized UV–Vis absorbance of **1** at 411 nm in decane/1,2-dichoroethane (99 : 1, *v*/*v*) at different monomer concentration: a) 0.04 mM; b) 0.05 mM; c) 0.06 mM; d) 0.07 mM. The solid lines denote Meijer–Schenning–van der Schoot mathematical fitting of the melting curves. The quantitative thermodynamic values are shown in **Table S2**.

Table S2. Thermodynamic parameters of 1 obtained by fitting temperature-dependent UV-Vis data.

1	0.04 mM	0.05 mM	0.06 mM	0.07 mM
T_e (K)	330.9	333.1	335.4	337.4
h_e (kJ mol^{-1})	–60.3	–62.3	–62.9	–59.5

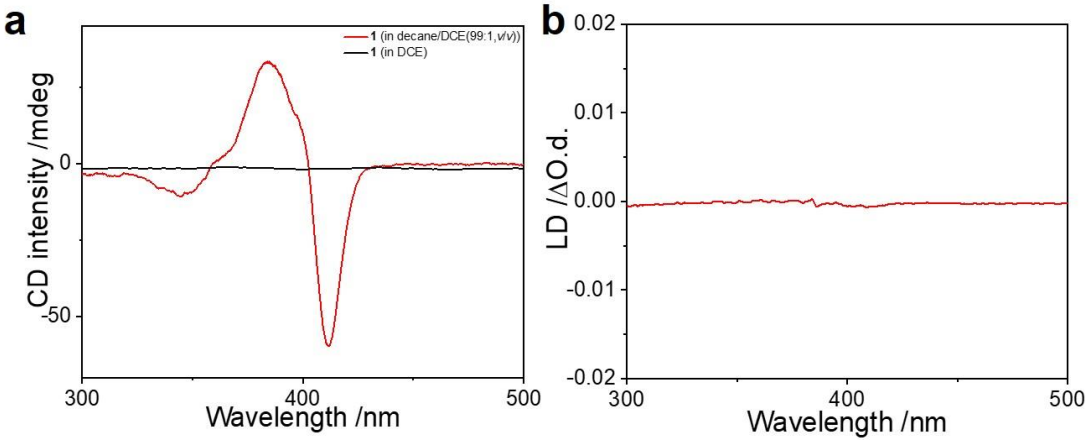

Figure S15. (a) CD spectra of **1** (c = 0.05 mM, 293 K, 5 mm cuvette) in 1,2-dichoroethane and decane/1,2-dichoroethane (99 : 1, *v*/*v*). (b) LD spectrum of **1** [0.05 mM in decane/1,2-dichoroethane (99 : 1, *v*/*v*), 293K]. As can be seen, no LD signal is detected, demonstrating the measured CD signals are real to reflect the supramolecular chirality.

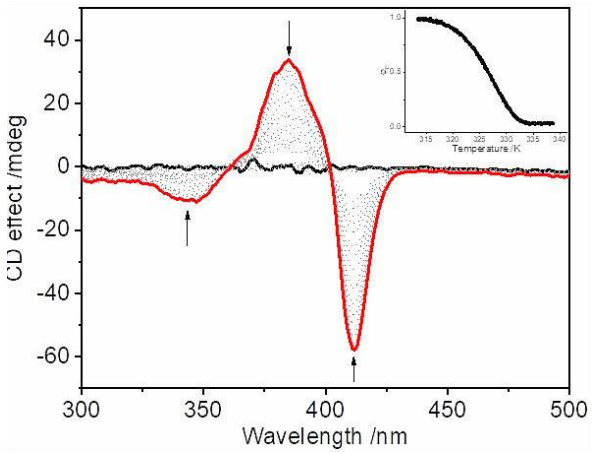

Figure S16. Temperature-dependent CD spectra of **1** in decane/1,2-dichoroethane (99 : 1, *v*/*v*). The arrows show spectral changes upon increasing the temperature. Inset: Normalized CD intensity of **1** at 411 nm *versus* temperature at a heating rate of 60 K h^{-1}. The non-sigmoidal melting curve indicates that **1** tends to adopt nucleation–elongation cooperative self-assembly mechanism, leading to the formation of one-dimensional supramolecular polymers at the aggregated state.

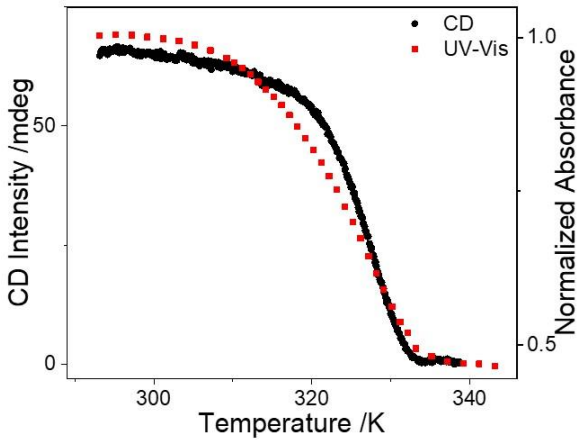

Figure S17. Overlapped normalized UV-Vis and CD intensity of **1** versus temperature in decane/1,2-dichoroethane (99 : 1, v/v, c = 0.05 mM) at a heating rate of 60 K h^{-1}.

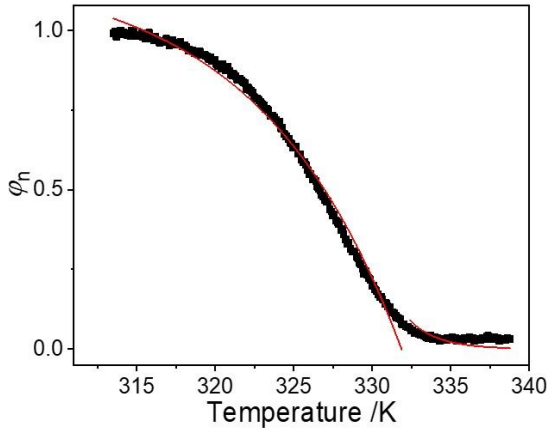

Figure S18. Normalized CD intensity of **1** at 411 nm *versus* temperature in decane/1,2-dichoroethane (99 : 1, *v*/*v*). The solid lines denote the mathematical fitting of the melting curve by the Meijer–Schenning–van der Schoot mathematical model. The quantitative thermodynamic values are shown in **Table 1**.

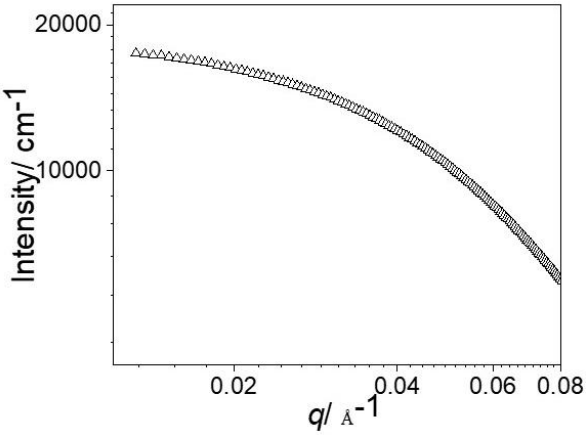

Figure S19. Plots of log I(*q*) *versus* log (*q*) of SAXS for **1** (0.1 mM in MCH). A q^{-1} slope is obtained in the region $0.03 < q < 0.08$ $Å^{-1}$, indicating the formation of one-dimensional rod-like structure upon supramolecular polymerization.

*4. Thermal hysteresis for supramolecular plymerization of **1–2***

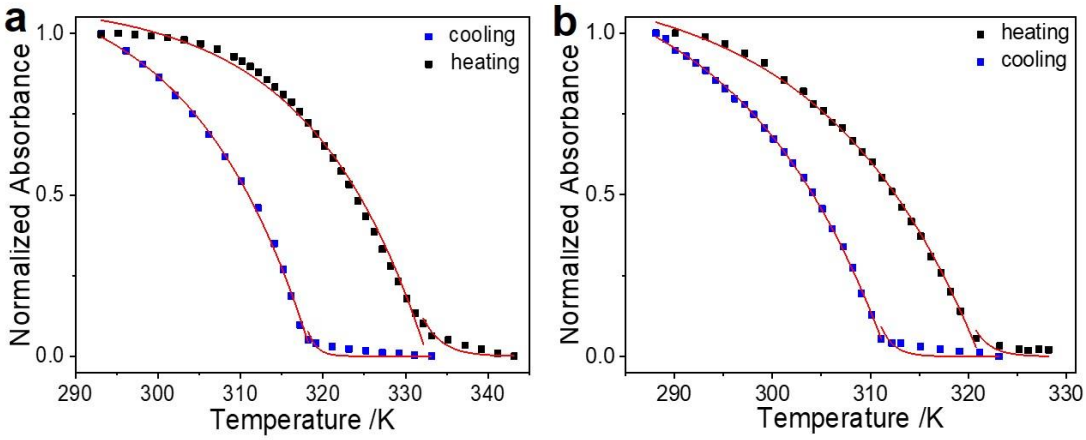

Figure S20. Normalized UV–Vis absorbance intensity of (a) **1** at 411 nm and (b) **2** at 358 nm *versus* temperature upon cooling (blue dots) and heating (black dots) at a rate of 60 K h^{-1}. Condition: c = 0.05 mM, decane/1,2-dichoroethane (99 : 1, *v/v*), 5 mm cuvette. The solid lines denote Meijer–Schenning–van der Schoot mathematical model fitting of the curves.

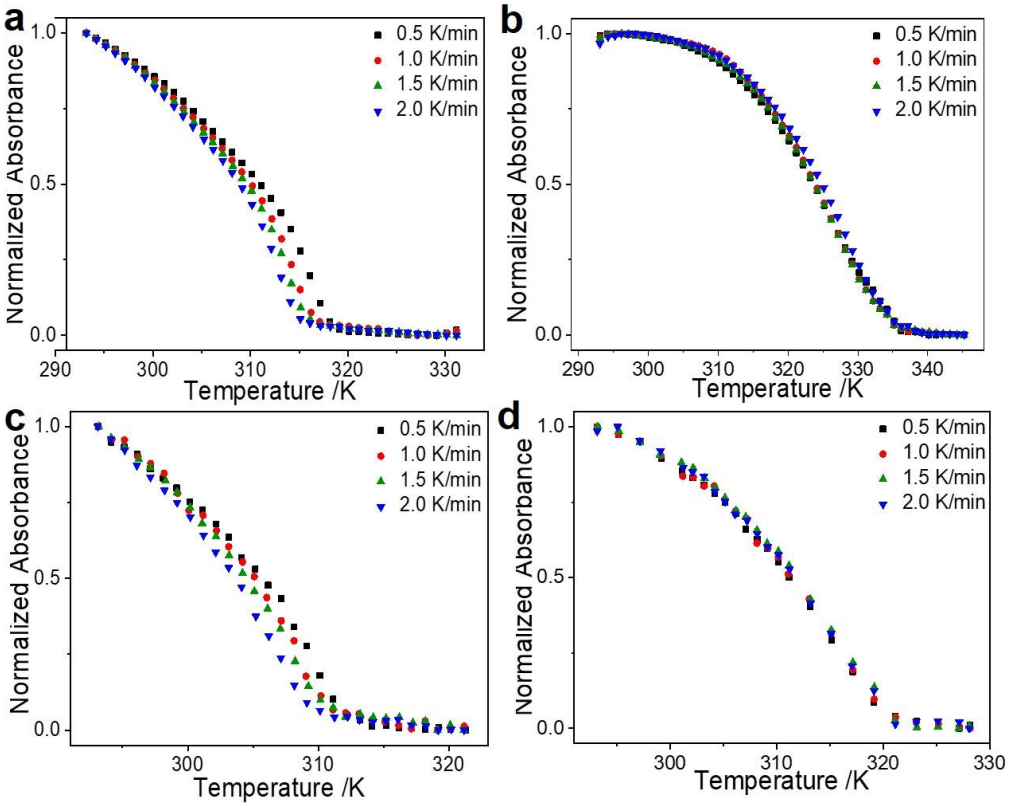

Figure S21. Normalized UV–Vis absorbance intensity of (a, b) **1** at 411 nm and (c, d) **2** at 358 nm *versus* temperature upon cooling (*left*) and heating (*right*) at different rates.

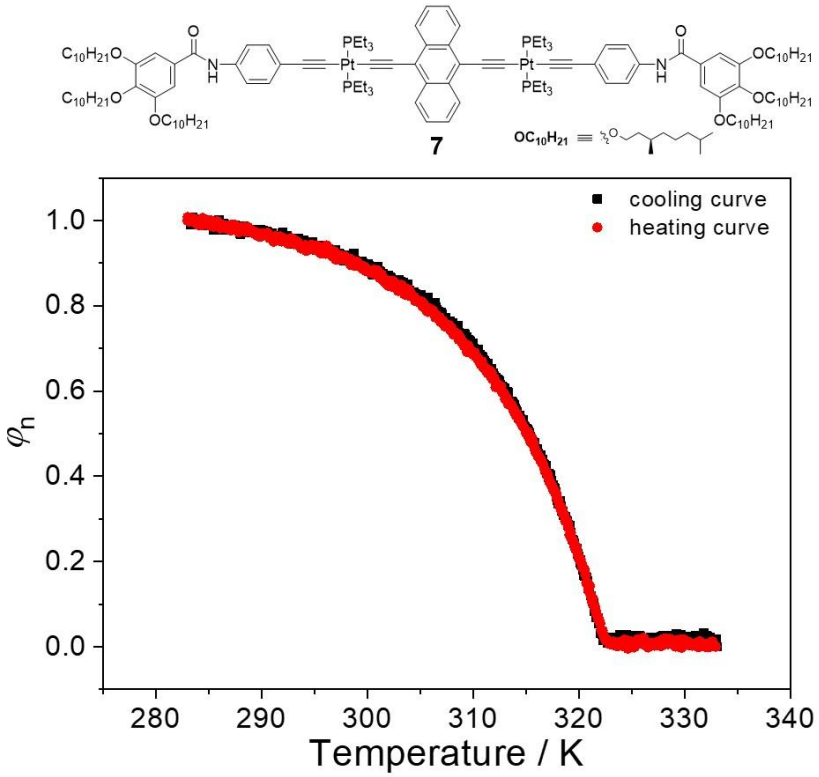

Figure S22. Normalized CD intensity of **7** at 489 nm *versus* temperature upon cooling (black dots) and heating (red dots) at a rate of 60 K h^{-1}. No hysteresis phenomenon is observed.

*5. Macroscopic gelation behaviors of **1–2***

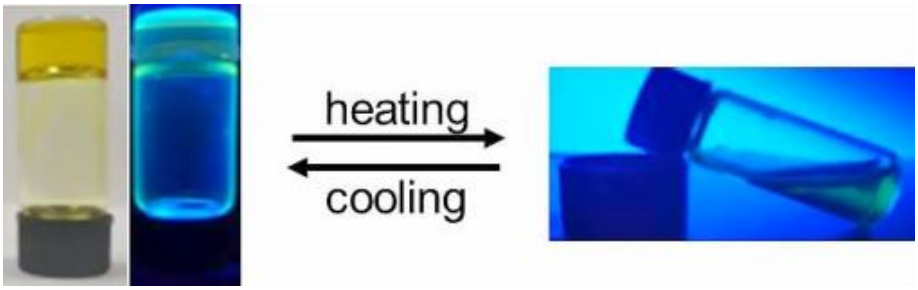

Figure S23. Thermo-responsive sol–gel transition of the supramolecular gels derived from **2.** The emission of supramolecular gels disappears upon heating, showing the "switching-on" emission charter.

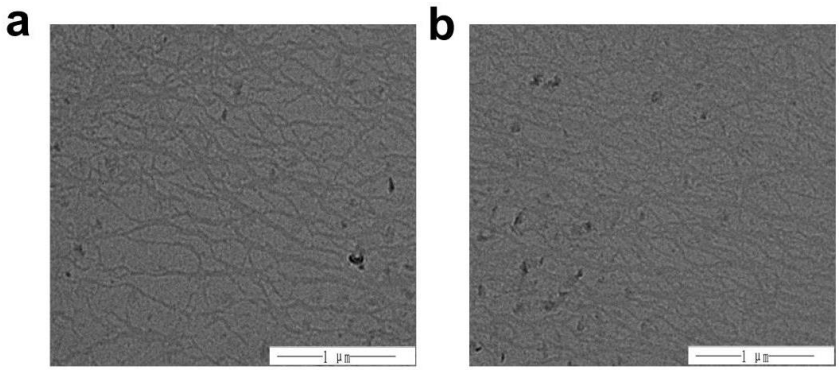

Figure S24. TEM images of (a) **1** and (b) **2** [copper grid, drop-casting from 0.40 mM solution in decane/1,2-dichoroethane (99 : 1, *v*/*v*)]. One-dimensional fibers are observed for **1** and **2**, laying the basis for the formation of three-dimensional supramolecular gels.

*6. Structural characterization of **1**–**2** and the synthetic intermediates*

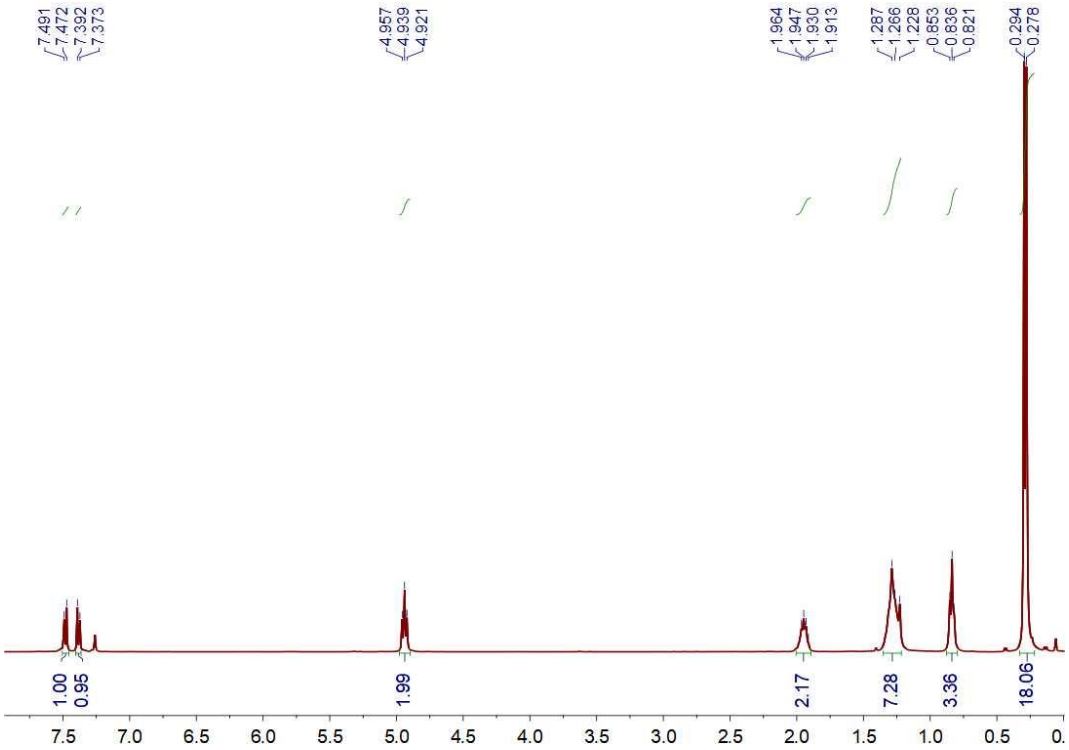

Figure S25. ^{1}H NMR spectrum (400 MHz, $CDCl_3$, 298 K) of **4a**.

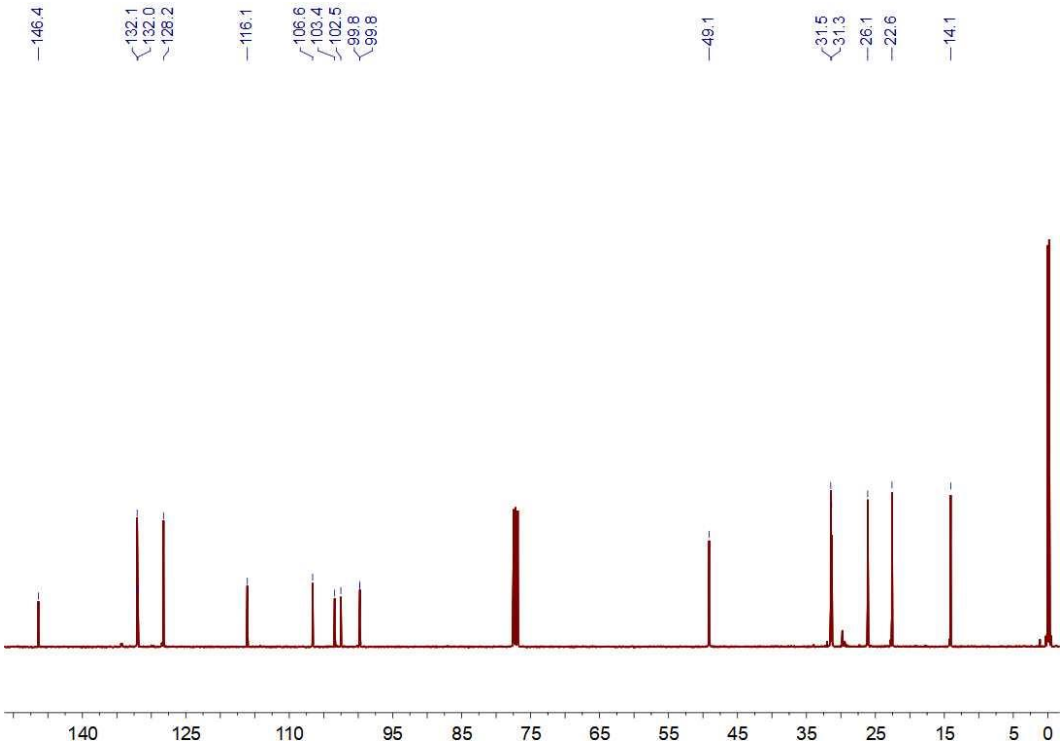

Figure S26. ^{13}C NMR spectrum (100 MHz, $CDCl_3$, 298 K) of **4a**.

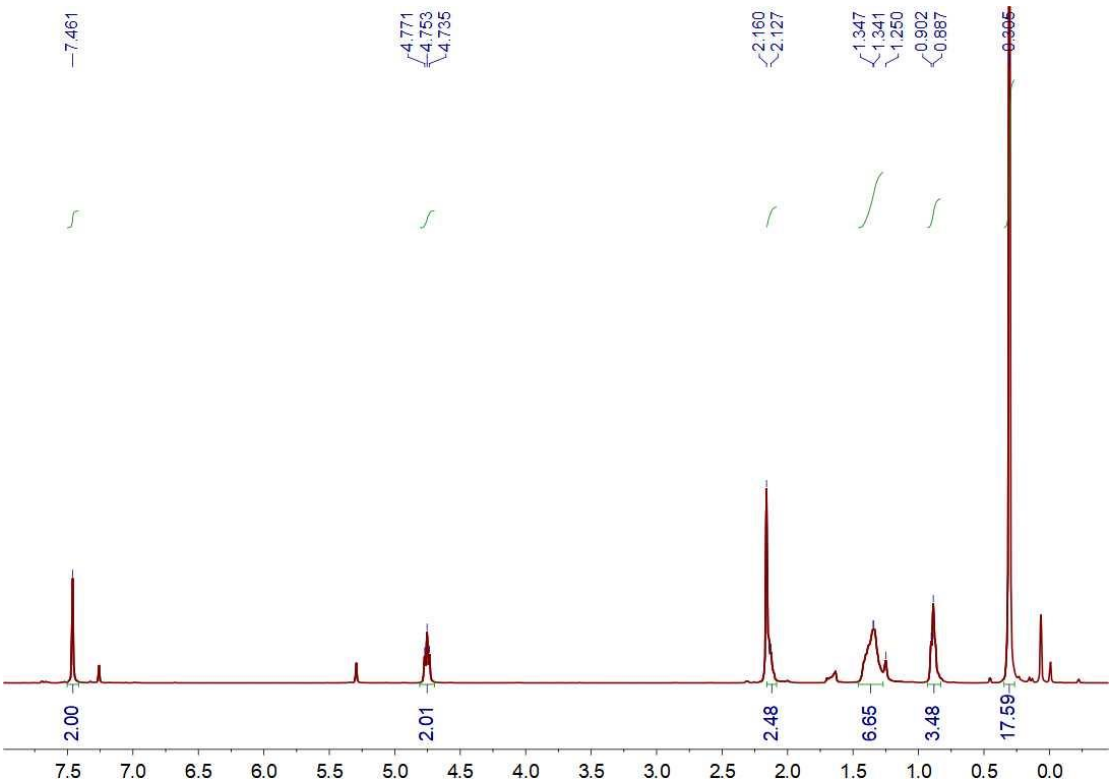

Figure S27. ^{1}H NMR spectrum (400 MHz, $CDCl_3$, 298 K) of **4b**.

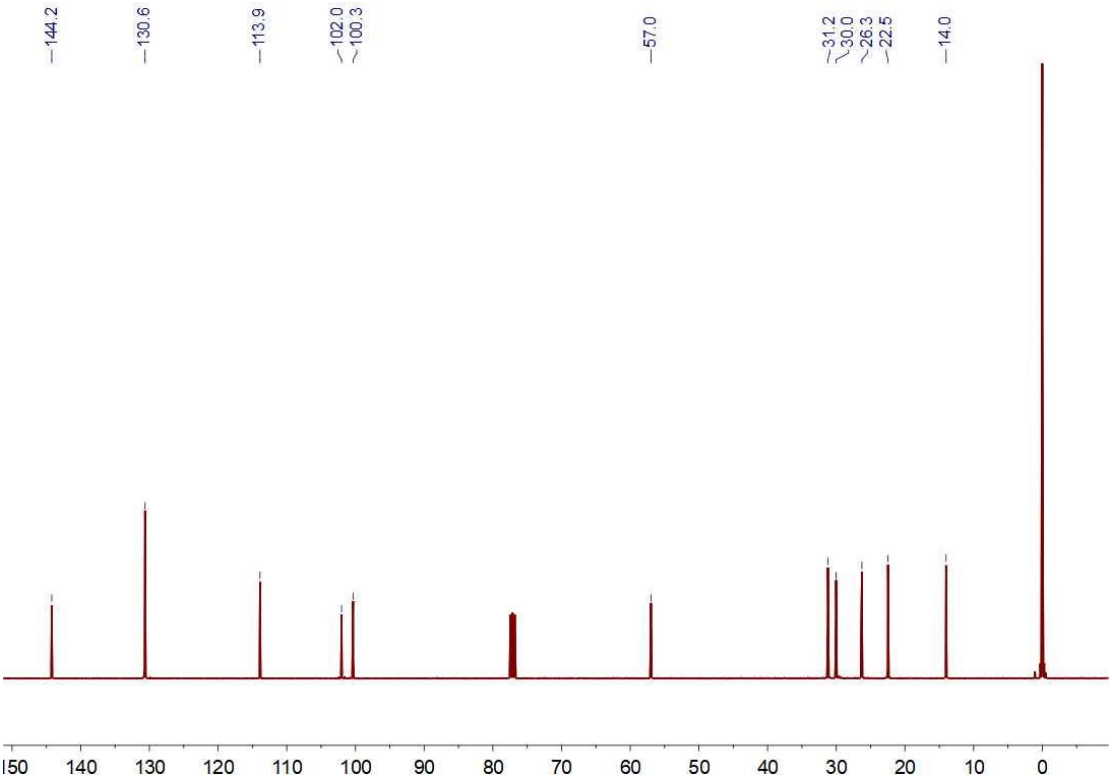

Figure S28. ^{13}C NMR spectrum (100 MHz, $CDCl_3$, 298 K) of **4b**.

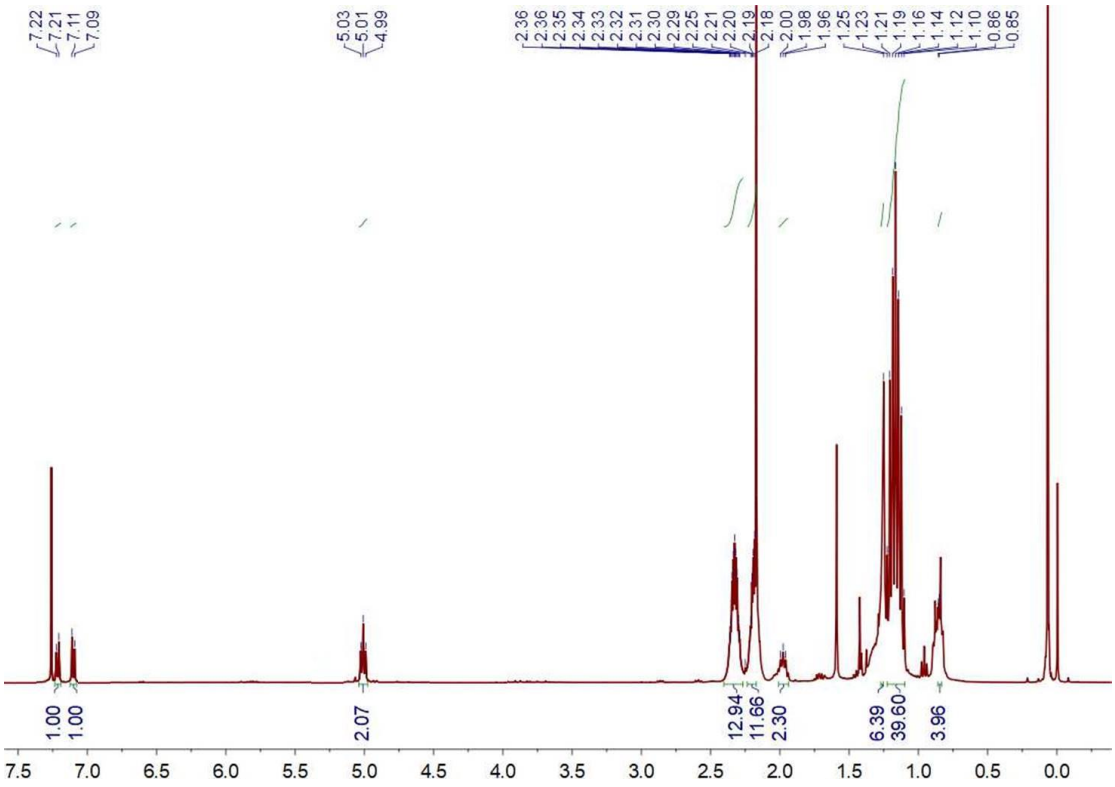

Figure S29. ^{1}H NMR spectrum (400 MHz, $CDCl_3$, 298 K) of **5a**.

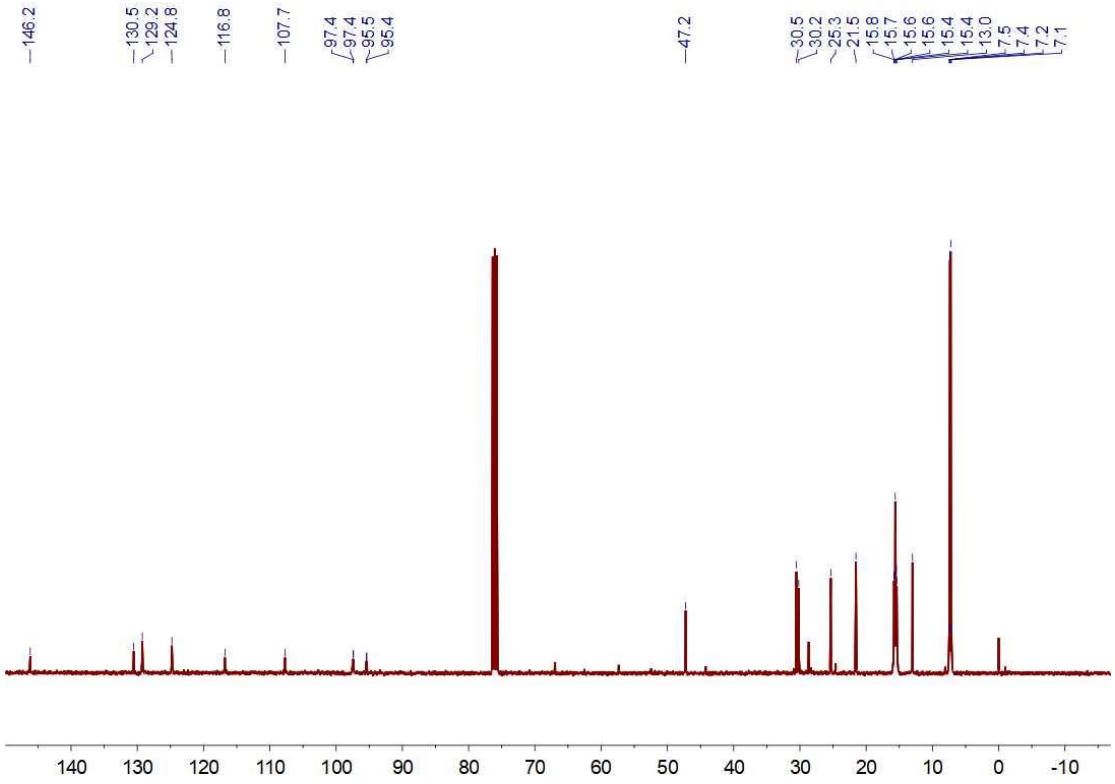

Figure S30. ^{13}C NMR spectrum (100 MHz, $CDCl_3$, 298 K) of **5a**.

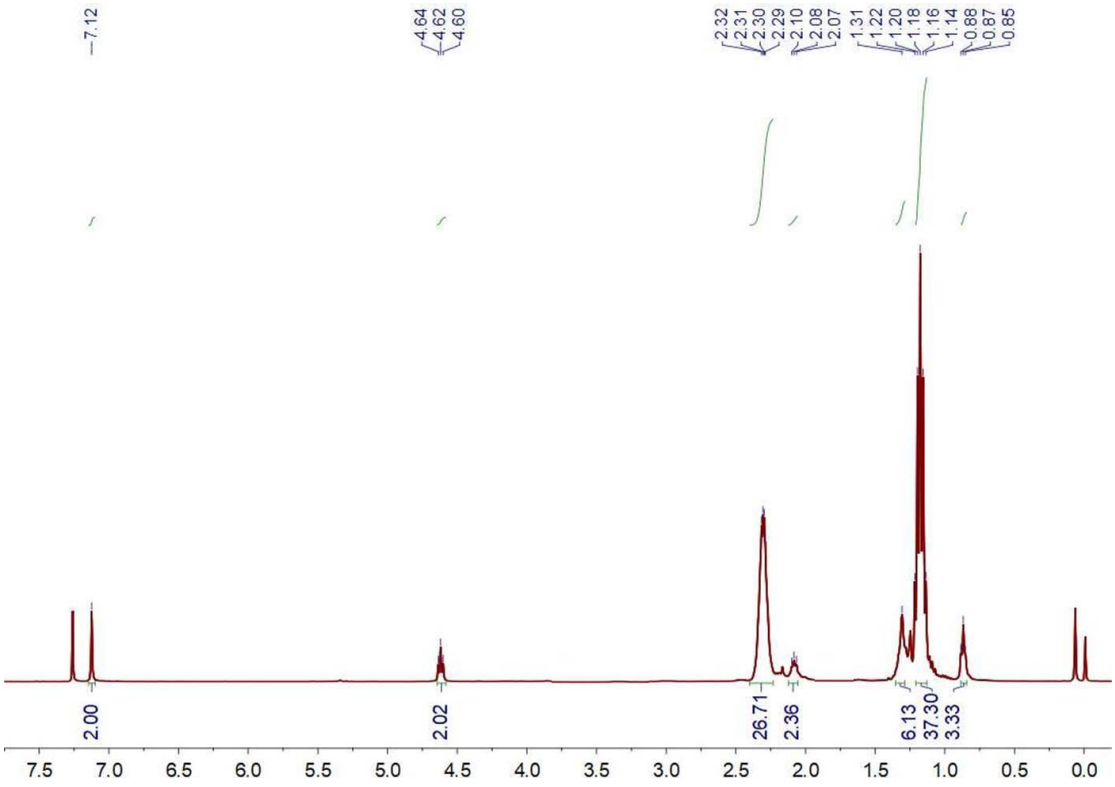

Figure S31. ^{1}H NMR spectrum (400 MHz, $CDCl_3$, 298 K) of **5b**.

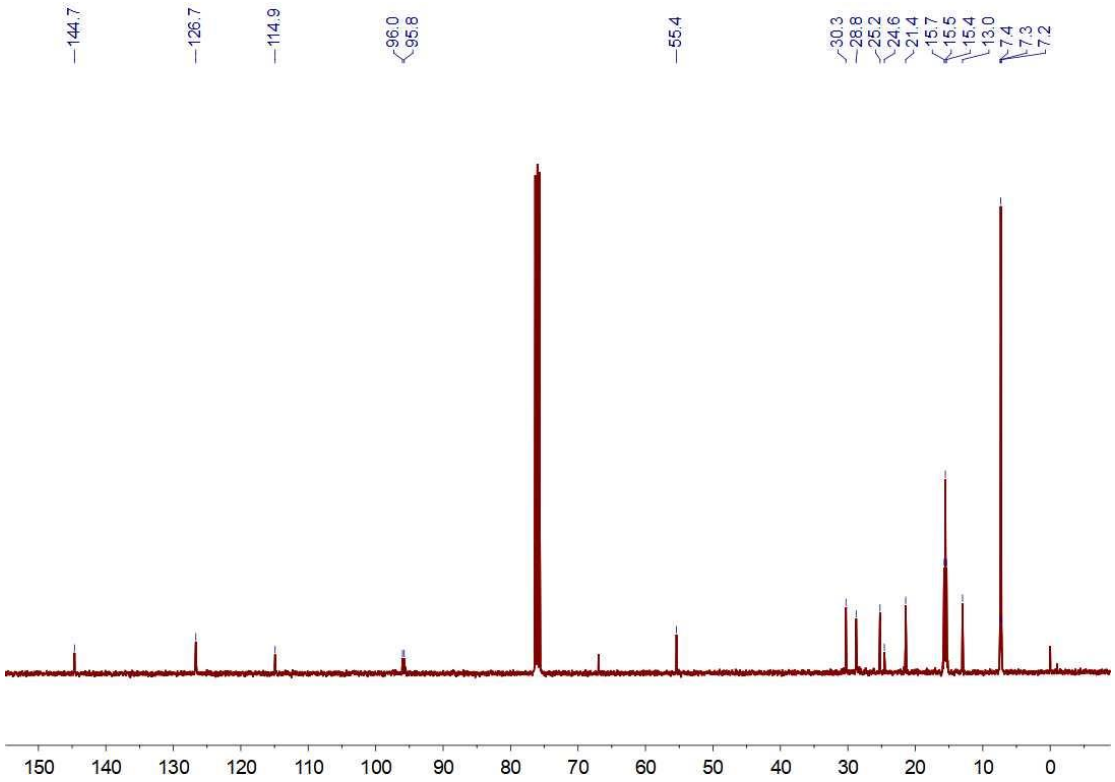

Figure S32. ^{13}C NMR spectrum (100 MHz, $CDCl_3$, 298 K) of **5b**.

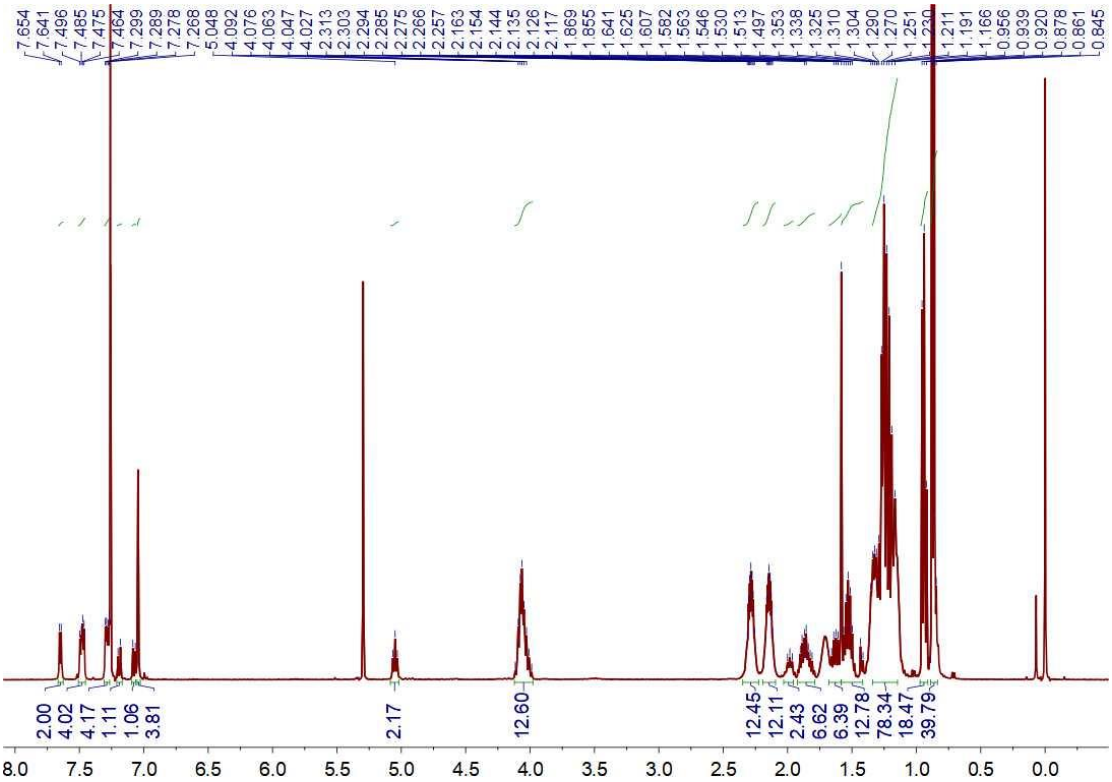

Figure S33. ^{1}H NMR spectrum (400 MHz, $CDCl_3$, 298 K) of **1**.

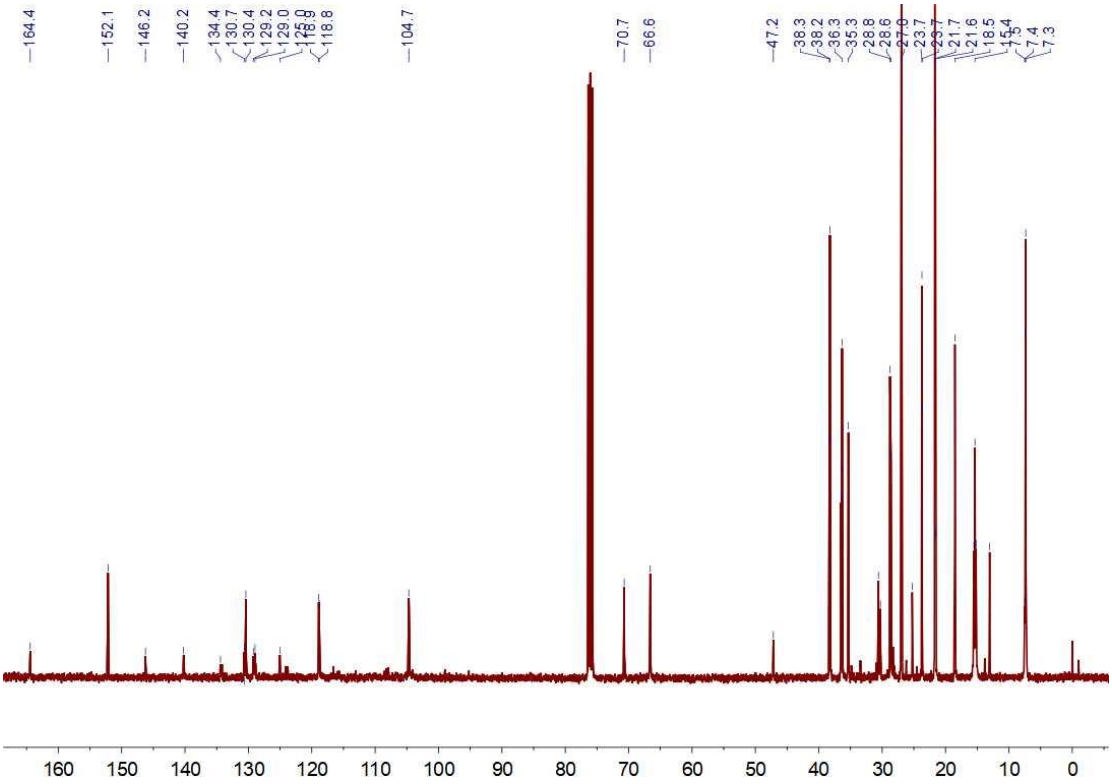

Figure S34. ^{13}C NMR spectrum (100 MHz, $CDCl_3$, 298 K) of **1**.

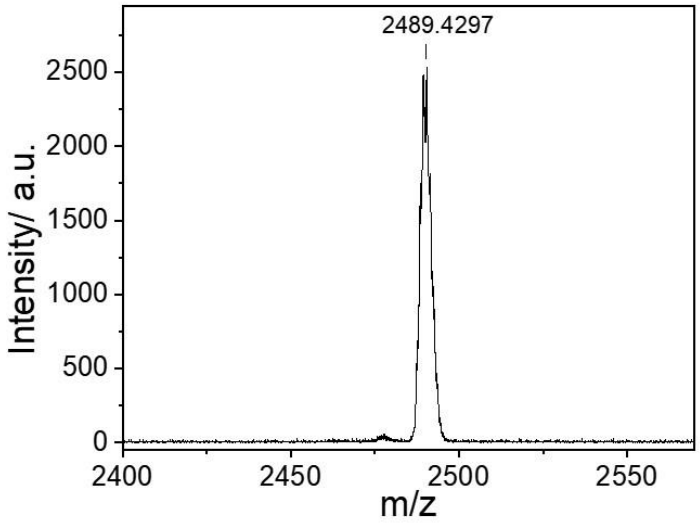

Figure S35. MALDI-TOF mass spectrum of **1**.

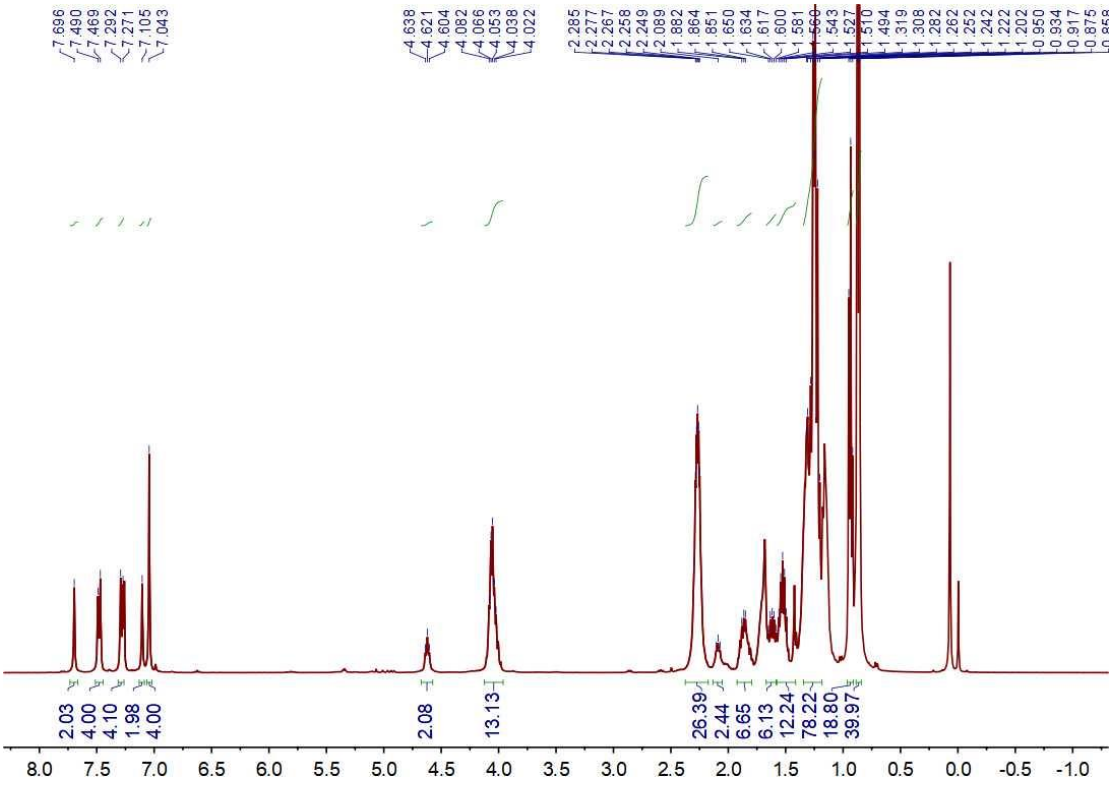

Figure S36. ^{1}H NMR spectrum (400 MHz, $CDCl_3$, 298 K) of **2**.

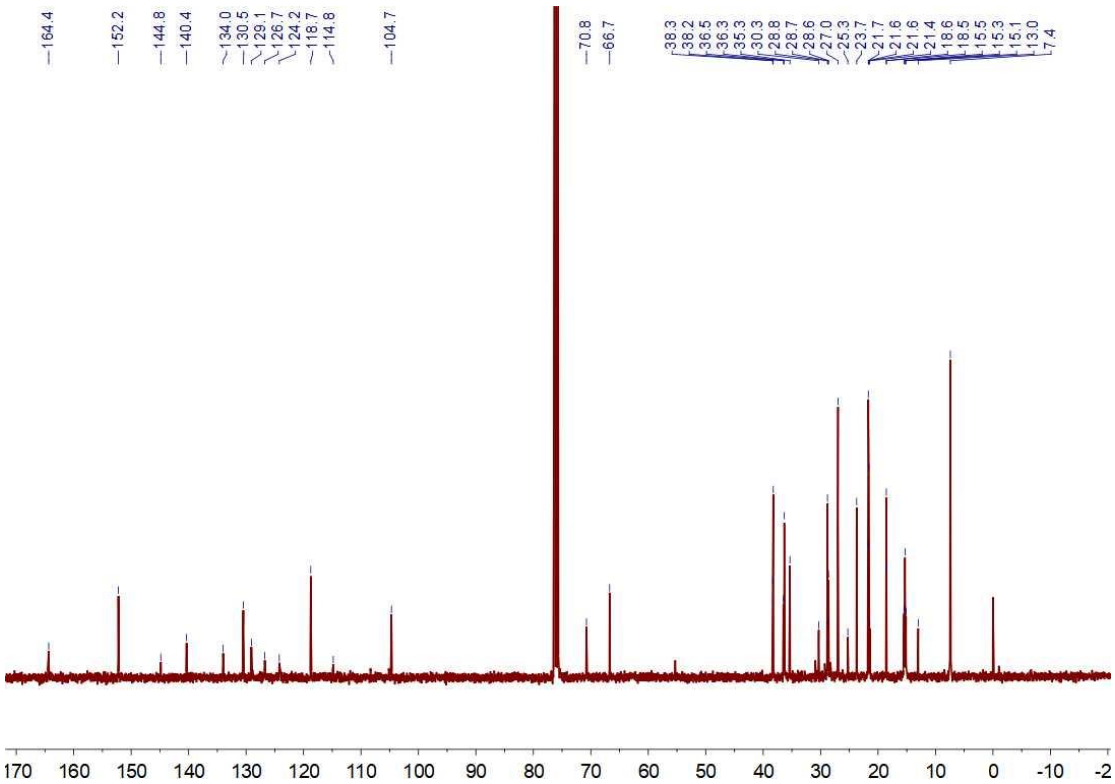

Figure S37. ^{13}C NMR spectrum (100 MHz, $CDCl_3$, 298 K) of **2**.

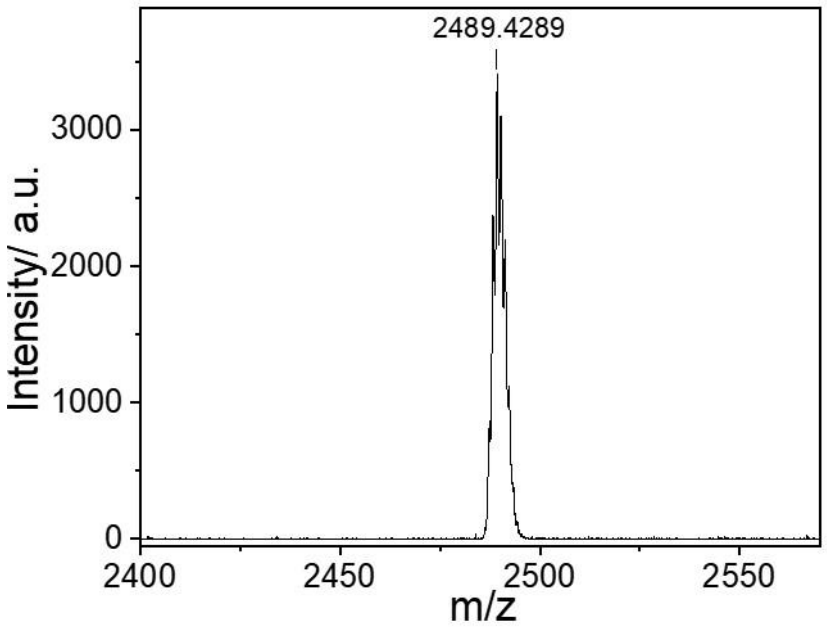

Figure S38. MALDI-TOF mass spectrum of **2**.